J Electr Eng Technol.2018; 13(5): 2050-2058
http://doi.org/10.5370/JEET.2018.13.5.2050

ISSN(Print) 1975-0102
ISSN(Online) 2093-7423

Investigation of Large-scale Transmission Tower Grounding Grid with High Amplitude and Uniform Flowing Impulse Current

Shuai Yang†, Jiarui Huang*, Shaodong Wei and Wenjun Zhou****

Abstract – Impulse characteristic of transmission tower grounding grid is needed for lightning protection of transmission line. This paper describes an outdoor experimental test facility established for large-scale grounding grid of transmission tower, made up of four impulse current generators and a circle current return electrode. The amplitude of impulse current is up to 100 kA. The results of the CDEGS simulation and GPR measurement reveal the uniform current distribution in the test arrangement. An impulse test for a square electrode with extended conductors is carried out in condition of three current waveforms with different amplitude. Based on the electrical network model and iterative algorithm method, a calculation model is proposed to simulate the impulse characteristic of large-scale grounding grid considering soil ionization. The curve of impulse resistance against the current amplitude shows the soil ionization both from the simulation and test. Deviation between the simulation and test result is less than 15%.

Keywords: Grounding grid, Impulse performance, Soil ionization, Iterative algorithm.

1. Introduction

Impulse performance of transmission tower grounding grid plays an important role in lightning protection of transmission line [1, 2]. Due to soil ionization and conductor inductance, impulse performance of grounding grid is quite different from that under power frequency condition [3, 4]. Numerical simulation and impulse test are two main investigation methods for the impulse characteristic of grounding grid. There are many kinds of simulation model applied with the development of computer technology [5-13]. But every model is based on some simplification and assumption, and the result need to be verified by lots of tests.

Current amplitude and grounding grid size are two main factors in the impulse test. Because of the limitation of test equipment, scale-down model of grounding grid with small current amplitude is widely used [14-16]. But there is no definite relationship between the scale-down model and the full-scale grounding grid. Limited test results on full-scale grounding grid in field test or at transmission towers have been publicized. In these tests, there is always a large-scale grounding grid with small current amplitude [17-21], or simple electrode with large current amplitude [22, 23]. Furthermore, the current return electrode is placed at one side or one point on a circle electrode. The current in these tests is flowing non-uniformly in the soil, which is inconsistent with the actual lightning current release process and affects the measurement result.

Thus this paper describes an outdoor experimental test facility established for large-scale grounding grid of transmission tower, which can generate a uniform flowing impulse current with amplitude up to 100 kA. Current distribution on the current return electrode is calculated using the CDEGS software in condition of different current generator arrangement. The GPR (ground potential rise) in the test area is measured along five paths. Based on this test facility, an impulse test for a square electrode with extended conductors is carried out. The test result is compared with the calculation model using electrical network model and iterative algorithm method, which takes soil ionization into consideration.

2. Test Facility for Large-scale Grounding Grid

2.1 Test facility arrangement

Four impulse current generators charging and discharging in parallel are used to generate high amplitude current. In order to make the impulse current flowing uniformly in the soil, a circle electrode with a diameter of 40 m is applied as the current return electrode. The tested grounding grid is buried at the center of the circle electrode. As shown in Fig. 1, four impulse generators are placed upon and connected with the circle electrode uniformly. The outputs of four generators are connected together in the circle center by overhead aluminum pipes. The impulse current is injected into the grounding grid buried in the circle center via a sphere gap, regulating impedance and current shunt. 60

† Corresponding Author: School of Electrical &Electronic Engineering, Hubei University of Technology, China. (ys3254@163.com)
* China Electric Power Research Institute Co., Ltd., China. (hjr947@foxmail.com)
** School of Electrical Engineering, Wuhan University, China. (wjzhou@whu.edu.cn)
Received: August 22, 2016; Accepted: April 4, 2018

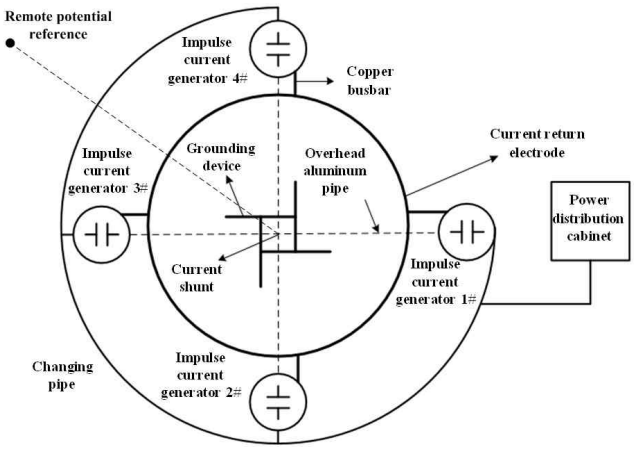

Fig. 1. Test facility arrangement

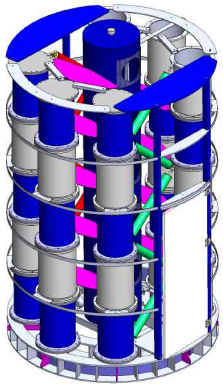

Fig. 2. Structure of an impulse current generator

mm×6 mm copper strip is the main material of the current return electrode which is buried in 1000 mm deep. In order to reduce the circuit resistance, 12 copper pipes are placed under the copper strip circle uniformly. The copper pipe is 1500 mm long, 3 mm thick and the radius is 25 mm.

Structure of a single impulse current generator is shown in Fig. 2. There are five capacitor banks in series and three pulse capacitors in parallel in one capacitor bank. The rated voltage of one capacitor is 200 kV and the rated capacitance is 0.6 μF. The tested grounding grid is a square electrode with extended conductors. The square side length is 4 m, and the conductor length is 4 m. The soil resistivity in the test area is 42.2 Ω·m, and the power-frequency grounding resistance of the tested grounding grid is 2.95 Ω. Based on the test arrangement above, three impulse currents are generated by changing the regulating impedance value. The front times and tail times of three impulse currents are 2.2 μs/24.5 μs, 4.7 μs/11 μs and 7.6 μs/18.5μs. The amplitude ranges are 5 kA-19 kA, 16 kA-100 kA, and 10 kA-53 kA respectively.

Impulse current is measured through a shunt with a resistance value of 0.0020684 Ω. The potential rise of the tested grounding grid and earth surface is measured by a capacitive voltage divider with a voltage division ratio of

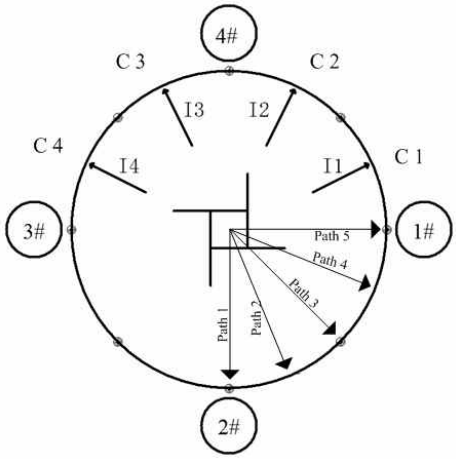

Fig. 3. Circular arcs division and GPR measurement paths for current distribution investigation

1051:1. The remote potential reference point is at the northwest corner 50 m far away from the circle center. The capacitive voltage divider is placed close to the tested grounding grid to reduce the length of measurement line connected to the high voltage terminal. The voltage measurement line connected to the remote potential reference point is a single insulated conductor supported by epoxy resin rods (1m tall), in a direction on the bisector of right angle formed by two current injection lines to minimize inductive coupling. TDS3014 digital oscilloscope is used to measure the current and potential rise waveform. The sampling rate is 1.25 GS/s, and the bandwidth is 100 MHz. The digital oscilloscope is powered by a UPS and placed on an insulation platform to be isolated from the high potential in the test.

2.2 Distribution of GPR and current in the test

Current distribution in the soil is unable to be measured, thus the current distribution on the current return electrode is calculated using the CDEGS software [24]. Because the test facility is symmetrical, just a semicircle is taken into consideration and divided into four circular arcs uniformly (C1-C4). The current distribution is calculated in case of one generator (#1), two generators (#1 and #3) and four generators. The current injected into the grounding grid is 2.6/50 μs with an amplitude of 20 kA. The result is shown in Fig. 4. The arrangement of current return electrode affects the current distribution significantly. Frequency domain analysis is applied in CDEGS simulation to obtain the result. The main frequencies of 2.6/50μs current are 0, 6.666, 13.333, 20.000, 26.667, 60.000, 93.333, 240.000, 480.000, 720.000, 960.000, 1200.000, 1440.000, 1680.000 and 1706.667 kHz. The current distribution result is composed with all those frequencies. For high-frequency content, current distribution is based on distributed circuit. Although the circle electrode is applied, the current is concentrated around the return point on the current return

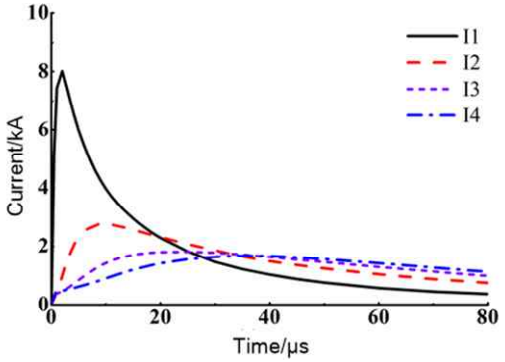

(a) Current distribution in case of one generator

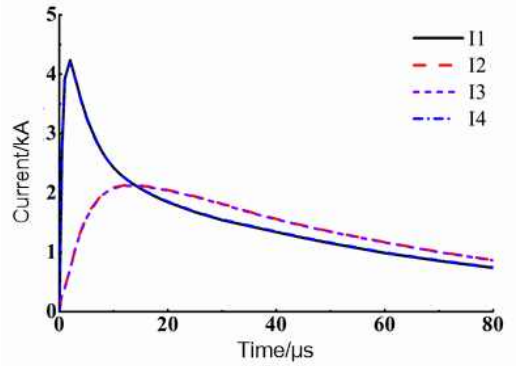

(b) Current distribution in case of two generators

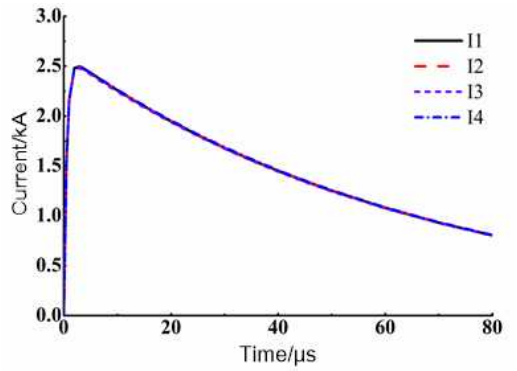

(c) Current distribution in case of four generators

Fig. 4. Current distribution on the return electrode based on CDEGS simulation

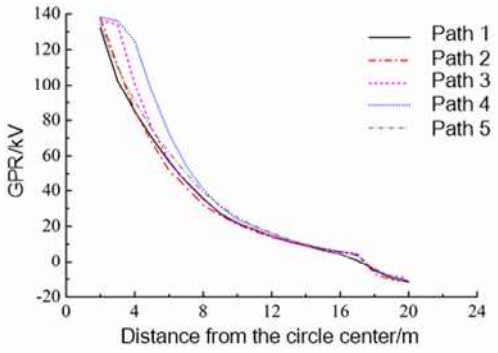

(a) GPR along five measurement paths

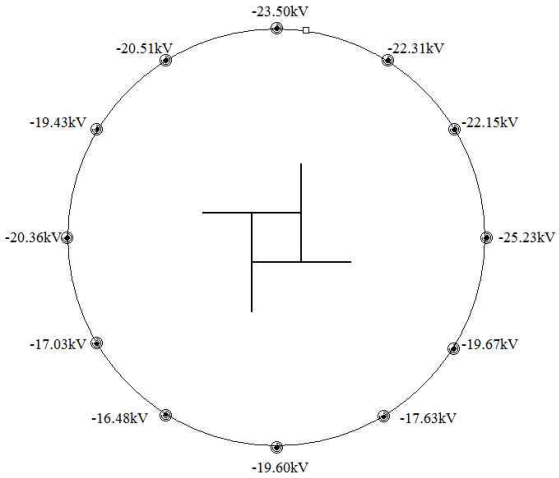

(b) Potential rise on current return electrode

Fig. 5. Potential rise of the current return electrode and along five measurement paths

electrode. The current is flowing non-uniformly as the return points are non-uniform. More generators placed uniformly could cause more uniform current distribution. According to the simulation result, current distribution is much uniform in case of four generators.

In order to reveal the current distribution indirectly, the potential rise of the current return electrode and the GPR along five paths in the test area are measured when 100 kA, 8/20 μs impulse current is injected into the grounding grid. The results are shown in Fig. 5. Current density in the soil affects the GPR distribution in the test. The GPR values along five paths are not consistent around the grounding grid due to higher current density around the conductor. As the distance of measurement point from the circle center increases, the effect of conductor is weakened and the difference of GPR values along five paths is much small. The potential rise of the circle electrode is not equipotential with the impulse current injected. The point connected with the generator is higher due to higher current density at the return point. Overall the potential rise distribution is uniform along different measurement paths, which reveal a uniform impulse current flowing in the test.

3. Simulation for Large-scale Grounding Grid

3.1 Grounding grid model

According to the electrical network model, a grounding grid is divided into several segments [13]. Each segment represents a branch of the circuit, made up of a serial resistance and self and mutual inductances. The response of this model is obtained though the frequency analysis. Fig. 6 shows a single horizontal grounding electrode divided into r segments and n nodes. The grounding grid is energized by injection of single frequency current at one or more nodes, named as $[F]_{n\times1}$. $[V]_{n\times1}$ is defined as the

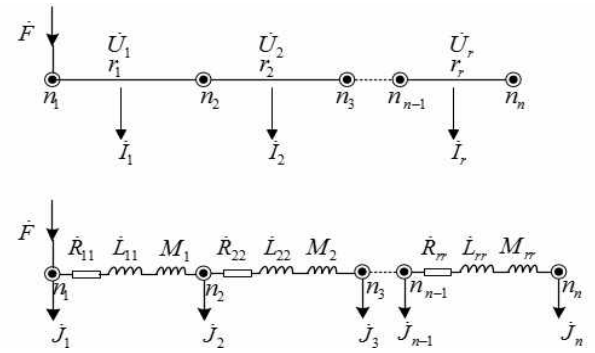

Fig. 6. Electrical network model of a single horizontal grounding electrode

voltage between each node and the remote potential reference, and $[U]_{r\times1}$ is the average voltage along each segment. As the segment is short enough, $[U]_{r\times1}$ is defined as the average of node voltages at a segment.

$$\bar{U}_{\mathrm{k}}=\frac{V_l+V_m}{2} \tag{1}$$

where l and m are two nodes in the both ends of segment k, and the following matrix equation is obtained.

$$[U]_{r\times1}=[\mathrm{k}]_{r\times n}\cdot[V]_{n\times1} \tag{2}$$

where $[k]_{r\times n}$ is the relation matrix of segments and nodes, and the elements are as follows.

$$k_{i,j}=\begin{cases}0.5 & \textit{when segment } l \textit{ is connected with node } m\\ 0 & \textit{when segment } l \textit{ isn't connected with node } m\end{cases}$$

There are two kinds of current in each segment, one is longitudinal current and the other is leakage current. The relationship between the leakage current $[I]_{\mathrm{r}\times1}$ and the respective voltage of each segment is shown as Eq. (3).

$$[I]_{r\times1}=[G]_{r\times r}\cdot[U]_{r\times1} \tag{3}$$

where $[G]_{\mathrm{r}\times\mathrm{r}}$ is a matrix of conductive and capacitive coefficients.

The longitudinal current in each segment is regards as a uniform one. The leakage current $[I]_{\mathrm{r}\times1}$ is assumed to just flow out of the nodes defined as $[J]_{\mathrm{n}\times1}$.

$$[J]_{r\times1}=[K]^{T}_{n\times r}\cdot[I]_{r\times1} \tag{4}$$

The single frequency current $[F]_{\mathrm{n}\times1}$ and leakage current $[J]_{\mathrm{n}\times1}$ at each node are regarded as current sources. According to nodal analysis, the following equation is acquired.

$$[F]_{n\times1}-[J]_{n\times1}=[Y]_{n\times n}\cdot[V]_{n\times1} \tag{5}$$

where $[Y]_{\mathrm{n}\times\mathrm{n}}$ is a matrix of the circuit including resistive and inductive effects.

Based on the equations above, following equation is obtained.

$$[F]_{n\times1}=\left([K]^{T}_{n\times r}\cdot[G]_{r\times r}\cdot[K]_{r\times n}+[Y]_{n\times n}\right)\cdot[V]_{n\times1} \tag{6}$$

The response of this model such as $[V]_{n\times1}$ and $[J]_{n\times1}$ can be calculated after the matrix $[G]_{r\times r}$ and $[Y]_{n\times n}$ are obtained.

3.2 Matrix $[Y]_{n\times n}$

$[Y]_{n\times n}$ is a matrix of the circuit, including self-resistance, self-inductance and mutual inductance. The self-resistance and self-inductance of segment j are obtained by Eqs. (7) and (8) respectively.

$$R_{jj}=\rho\frac{l}{s} \tag{7}$$

$$L_{jj}=\frac{\mu}{2\pi}\left(\ln\frac{2r}{l}-1\right) \tag{8}$$

where l is the segment length; s is the segment sectional area; r is conductor radius; μ is magnetic permeability of soil; ρ is conductor resistivity.

The mutual inductance of segment j and segment k is acquired as follows.

$$L_{jk}=\frac{\mu}{4\pi}\int_{l_j}\int_{l_k}\frac{dl_k\cdot dl_j}{d_{jk}} \tag{9}$$

where d_{jk} is the distance between d_j and d_k.

According to these equations above, the branch admittance matrix of the model is obtained. $[Y]_{n\times n}$ is calculated as follows.

$$Y=AY_bA^{T} \tag{10}$$

where $[A]$ is the relation matrix of model.

3.3 Matrix $[G]_{r\times r}$

Based on Eq. (3), following equation is obtained.

$$[U]_{r\times1}=[Z]_{r\times r}\cdot[I]_{r\times1} \tag{11}$$

where $[Z]_{r\times r}$ is transposed matrix of $[G]_{r\times r}$.

Element Z_{jk} in matrix $[Z]_{r\times r}$ represents the potential rise in segment j when one unit current is drained in segment k. This paper only introduces the calculation in homogeneous soil, while mirror image method is applied in condition of multilayer soil. Segment length cannot be neglected for reducing the calculation error. A segment must be divided as multiple units. One unit current is drained in segment k, and the segment length is l_{k}. dl_{k} is one unit on segment k,

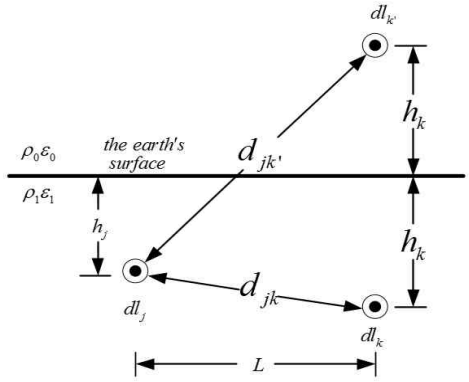

Fig. 7. Mirror image of current source

and the current drained from dl_k is dl_k/l_k. The length of segment j is l_j, and dl_j is one unit on it. Taking the surface of earth into account, a mirror image of current source dl_k should be added as $\alpha dl_k/l_k$ in Fig. 7. α is the mirror image coefficient of soil to air. For a single frequency current, the current density could be expressed as follows.

$$J = \sigma E + j\omega\varepsilon E \tag{12}$$

The mirror image coefficient of soil to air could be acquired as follows.

$$\sigma = \frac{1/\rho_1 - 1/\rho_0 + j\omega(\varepsilon_1 - \varepsilon_0)}{1/\rho_1 + 1/\rho_0 + j\omega(\varepsilon_1 + \varepsilon_0)} \tag{13}$$

where ρ_0 is the resistivity of air, Ω·m; ε_0 is the permittivity of air, F/m; ρ_1 is the resistivity of soil, Ω·m; ε_1 is the permittivity of soil, F/m; ω is the angular frequency of single frequency current, rad/s.

Air resistivity is assumed to be infinite, and Eq. (13) is simplified as follows.

$$\sigma = \frac{1/\rho_1 + j\omega(\varepsilon_1 - \varepsilon_0)}{1/\rho_1 + j\omega(\varepsilon_1 + \varepsilon_0)} \tag{14}$$

The potential rise of dl_j on segment j caused by current source dl_k and its mirror image $\alpha dl_k/l_k$ is acquired as follows.

$$dU_{jk} = \frac{1}{4\pi(1/\rho_1 + j\omega\varepsilon_1)}\left(\frac{dl_k/l_k}{dj_k} + \alpha\frac{dl_k/l_k}{d_{jk'}}\right) \tag{15}$$

$$d_{jk} = \sqrt{L^2 + (h_k - h_j)^2} \tag{16}$$

$$d_{jk'} = \sqrt{L^2 + (h_k + h_j)^2} \tag{17}$$

where d_{jk} is the distance between dl_k and dl_j, m; $d_{jk'}$ is the distance between mirror image $dl_{k'}$ and dl_j, m; L is the horizontal distance between $dl_{k'}$ and dl_j, m.

The average potential rise of segment j caused by segment k is obtained as follows.

$$U_{jk} = \frac{1}{4\pi(1/\rho_1 + j\omega\varepsilon_1)l_k l_j}\int_{l_j}\int_{l_k}\left(\frac{1}{d_{jk}} + \alpha\frac{1}{d_{jk'}}\right)dl_k dl_j \tag{18}$$

Thus the element Z_{jk} in matrix $[Z]_{r\times r}$ is obtained by Eq. (19).

$$Z_{jk} = \frac{1}{4\pi(1/\rho_1 + j\omega\varepsilon_1)l_k l_j}\int_{l_j}\int_{l_k}\left(\frac{1}{d_{jk}} + \alpha\frac{1}{d_{jk'}}\right)dl_k dl_j \tag{19}$$

Based on the same method, diagonal elements of the matrix are obtained as follows.

$$Z_{jj} = \frac{1}{2\pi(1/\rho_1 + j\omega\varepsilon_1)l_j}\left(\frac{1}{2l_j}\int_{l_j}\int_{l_{j'}}\frac{\alpha}{d_{jj'}}dl_{j'}dl_j + \frac{r}{l_j} + \ln\frac{l_j + \sqrt{l_j^2 + r^2}}{r} - \sqrt{1 + (\frac{r}{l_j})^2}\right) \tag{20}$$

where r is the radius of segment j, m.

3.4 Iterative algorithm of soil ionization

Soil ionization takes place when the current leaking into the earth is high enough to produce electric field intensity greater than a critical value, which is defined as soil ionization. In order to take the soil ionization into consideration, the equivalent radius of grounding grid is applied [12]. The conductor segment of grounding grid is modeled using cylindrical conductor and its equivalent radius r_i is increased after the soil ionization occurs according to the following equations.

$$r_i = \frac{rE}{E_c} \tag{21}$$

$$E = \frac{I_i}{2\pi l_i r(1/\rho + j\omega\varepsilon)} \tag{22}$$

where r_i is the equivalent radius of segment i, m; I_i is the leakage current of segment i, kA; ρ is the resistivity of soil, Ω·m; l_i is the length of segment i, m; E_c is the critical breakdown strength of soil, kV/m; r is the radius of grounding conductor, m.

According to the calculation of matrix $[G]$ and $[Y]$, the diagonal element of matrix $[G]$ varies with the change of equivalent radius, and matrix $[Y]$ remains unchanged. Leakage current is needed to obtain the equivalent radius, and it also varies with the equivalent radius. Thus the iterative algorithm is applied to build up the relation between equivalent radius and leakage current. Firstly as the frequency of current is ω, $[F(\omega)]$ is obtained by means of Fourier transform, $[Y(\omega)]$ and $[G(\omega)]$ are calculated according to the initial parameters of the grounding grid. Then the response matrix is computed based on the method above such as $[U(\omega)]$, $[V(\omega)]$, $[I(\omega)]$ and $[J(\omega)]$. The time

dependent response is obtained lately. According to the leakage current I_i of segment i, the equivalent radius r_i of segment i increased by the soil ionization is obtained by Eqs. (22) and (23). This equivalent radius r_i is used to calculate the variation matrix of leakage current at the node, named as $[\Delta J(\omega)]$. Superimposing $[\Delta J(\omega)]$ on $[F(\omega)]$ as new external current source, the response matrix is computed again. The iterative algorithm is finished until convergence criterion is achieved.

4. Comparison between Test and Simulation

The critical breakdown field strength of soil is measured using a coaxial cylindrical electrode [25], and the value ranges from 210 kV/m to 280 kV/m. According to the grounding grid size and soil parameter, impulse characteristic of the tested grounding grid is simulated using the method proposed. The soil resistivity is 42.2 Ω·m and the soil relative permittivity is 10. The large-scale test is carried out in condition of three impulse current waveforms. Impulse grounding resistance and potential rise are shown in Fig. 8 and Fig. 9 respectively.

The impulse grounding resistance obtained from the proposed model is consistent with the test result. Compared with measured value, calculation error of the method is less than 15%. The curve of impulse resistance against the current amplitude shows the soil ionization both from the

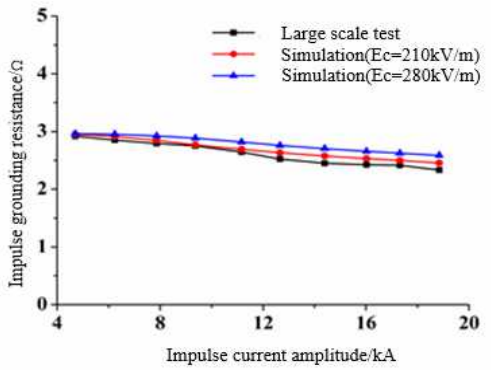

(a) 2.2μs/24.5μs

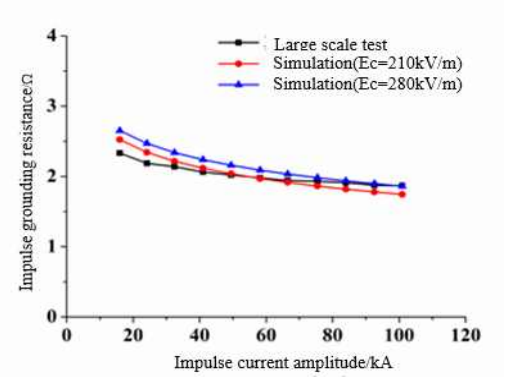

(b) 4.7μs/11μs

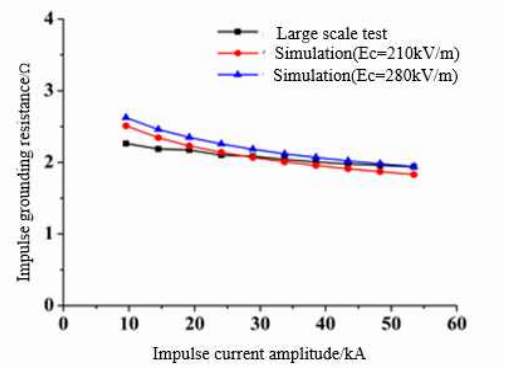

(c) 7.6μs/18.5μs

Fig. 8. Impulse grounding resistance against current amplitude in case of different current waveforms

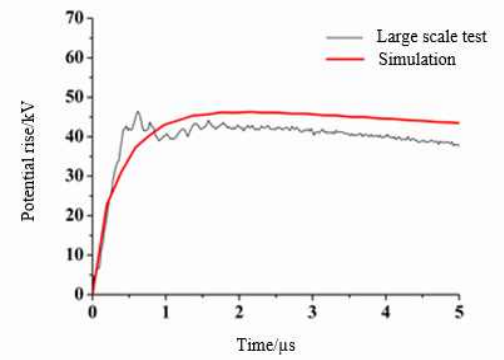

(a) 2.2μs/24.5μs/19kA

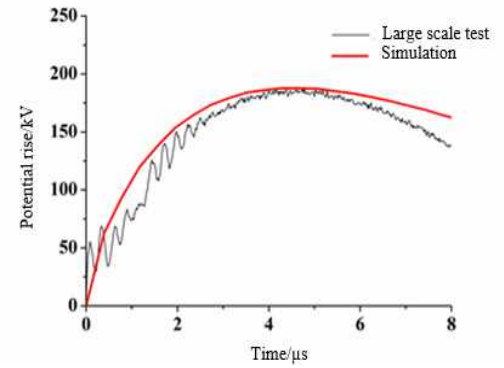

(b) 4.7μs/11μs/100kA

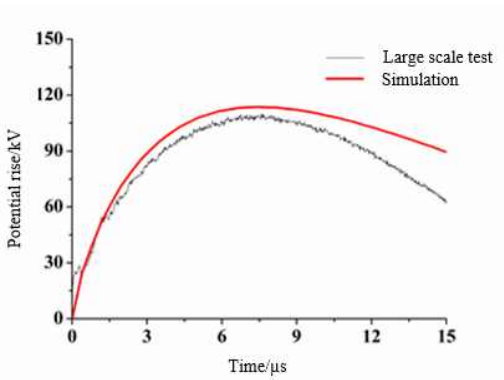

(c) 7.6μs/18.5μs/54kA

Fig. 9. Potential rise in case of different current waveforms

model and test. Impulse grounding resistance decreases with the increase of impulse current amplitude. But the decrease trend is not obvious due to the low soil resistivity and large grounding grid size. Large size reduces the current density around the grounding grid, and low soil resistivity leads to low electric field intensity around the grounding grid. The current amplitude is up to 100 kA in case of 4.7 μs/11 μs current waveform, but the impulse grounding resistance decreases non-significantly when the current amplitude exceeds 60 kA. The wave front of grounding potential rise is obtained from the model and test. The waveform calculated is smooth and the variation tendency is consistent with that of test. The waveform measured shows obvious oscillation due to the refraction and reflection of wave propagation in the long measurement circle.

Soil parameters are important in the simulation such as soil resistivity, permittivity and critical breakdown field strength. Critical breakdown field strength of soil is not the same in published literatures, and the main value is about 300-400 kV/m [26]. Comparison between 210 kV/m and 280 kV/m reveals that critical breakdown field strength affect simulation result. As the injection current is small, leakage current of conductor segment is small which cause low electric field intensity on the conductor surface. The effect of soil ionization and critical breakdown field strength is not significant in condition of small current. As the current increases, effect of critical breakdown field strength is obvious. Higher critical breakdown field strength leads to larger impulse grounding resistance. The variation trends of impulse grounding resistance against current amplitude with different critical breakdown field strength are consistent. This is because the equivalent radius of segment is inversely linked to critical breakdown field strength based on Eq. (21). In order to obtain accurate simulation result, critical breakdown field strength of soil needs to be measured for certain researched object.

According to reference [4, 27, 28], the soil resistivity and permittivity are dependent on the frequency as follows.

$$\rho = \rho_0 \left\{1+\left(1.2\times10^{-6}\times\rho_0^{\,0.73}\right)\times\left[\left(f-100\right)^{0.65}\right]\right\}^{-1} \quad (23)$$

$$\varepsilon = 7.6\times10^{3}\times f^{-0.65}+1.3 \quad (24)$$

In the model proposed in this paper, the soil parameter is assumed to be constant value. The consistency between test and simulation is good. If the frequency dependent soil parameter is applied, the matrix $[G]_{r\times r}$ and $[Y]_{n\times n}$ needs to be recalculated at each single frequency current. Furthermore electric field intensity on the conductor surface is also modified at each single frequency according to Eqs. (21) and (22). Those two modifications make much more calculation amount in the iterative algorithm comparatively to the condition of constant soil parameter. Frequency dependent soil resistivity decreases the potential rise value in reference [27, 28]. According to the comparison between the test and simulation in this paper, simulation result is a little larger than that of test. Thus the frequency dependent soil parameter might reduce the calculation error. Simplification and optimization of the model proposed will be carried out in following research.

This paper proposes a test facility and a simulation model for large-scale grounding grid of transmission tower. The test facility is built up not only for investigation but also for industry application. Based on the test facility, impulse performance of different grid structure is estimated in testing environment much closer to the actual lightning process. Furthermore some new material of grounding grid can be tested such as graphite electrode. Due to the immovability of the test facility, it cannot be used for estimating the actual grounding grid. The simulation is proposed for extending the estimation, and the comparison between test and simulation reveals good consistency for application.

5. Conclusion

1) A test facility is built up to generate a uniform flowing impulse current with the amplitude up to 100 kA. Four impulse current generators charging and discharging in parallel are placed upon a circle current return electrode with a diameter of 40 m. The results of the CDEGS simulation and GPR measurement reveal the uniform current distribution in the test.

2) The curve of impulse resistance against the current crest value shows the soil ionization in the test. Impulse grounding resistance decreases with the increase of impulse current amplitude. But the decrease trend is not obvious due to the low soil resistivity and large grounding grid size. Large size reduces the current density around the grounding grid, and low soil resistivity leads to low electric field intensity around the grounding grid.

3) Based on electrical network model and iterative algorithm, this paper proposes a model to simulate the impulse characteristic of large-scale grounding grid. Compared with measured value, calculation error is less than 15%.

Acknowledgements

This work was supported by the National Natural Science Foundation of China (51277136).

References

[1] A. Geri, "Behavior of Grounding Systems Excited by High Impulse Currents: The Model and Its Validation," *IEEE Trans. Power Del.*, vol. 14, no. 3, pp. 1008-1017, Jul. 1999.

[2] A. Habjanic and M. Trlep, "The simulation of the soil ionization phenomenon around the grounding system by the finite element method," *IEEE Trans. Magn.*, vol. 42, no. 4, pp. 867-870, Apr. 2006.

[3] L. Grcev and F. Menter, "Transient Electromagnetic Fields Near Large Earthing Systems," *IEEE Trans. Magn.*, vol. 12, no. 3, pp. 1525-1528, May 1996.

[4] S. Visacro, R. Alipio, M. Vale, and C. Pereira, "The Response of Grounding Electrodes to Lightning Currents: The Effect of Frequency Dependent Soil Resistivity and Permittivity," *IEEE Trans. Electromagn. Compat.*, vol. 52, no. 2, pp. 401-406, May 2011.

[5] F. Menter and L. Grcev. "EMTP-Based Model for Grounding System Analysis," *IEEE Trans. Power Del.*, vol. 9, no. 4, pp. 1838-1849, Oct. 1994.

[6] A. Geri, G. M. Veca, E. Garbagnati and G. Sartorio, "Non-linear Behavior of Ground Electrodes Under Lightning Surge Currents: Computer Modeling and Experimental Results," *IEEE Trans. Magn.*, vol. 28, no. 2, pp. 1442-1445, Mar. 1992.

[7] B. Zhang, J. He, J. Lee, X. Cui, Z. Zhao, J. Zou and S. Chang, "Numerical analysis of transient performance of grounding systems considering soil Ionization by coupling moment method with circuit theory," *IEEE Trans. Magn.*, vol. 41, no. 5, pp. 440-1443, May 2005.

[8] B. Nekhoul, C. Guerin, P. Labie, G. Meunier, R. Feuillet and X. Brunotte, "A Finite Element Method for Calculating the Electromagnetic Fields Generated by Substation Grounding Systems," *IEEE Trans. Magn.*, vol. 31, no. 3, pp. 2150-2153, May 1995.

[9] S. Sekioka, M. I. Lorentzou, M. P. Philippakou and J. M. Prousalidis, "Current-Dependent Grounding Resistance Model Based on Energy Balance of Soil Ionization," *IEEE Trans. Power Del.*, vol. 21, no. 1, pp. 194-201, Jan. 2006.

[10] B. Zhang, J. W., J. He and R. Zeng, "Analysis of transient performance of grounding system considering soil ionization by time domain method," *IEEE Trans. Magn.*, vol. 49, no. 5, pp. 1837-1840, May 2013.

[11] Z. Feng, X. Wen, X. Tong, H. Lu, L. Lan and P. Xing, "Impulse Characteristics of Tower Grounding grids Considering Soil Ionization by the Time Domain Difference Method," *IEEE Trans. Power Del.*, vol. 30, no. 4, pp. 1906-1913, Aug. 2015.

[12] J. Cidrás, A. F. Otero and C. Garrido, "Nodal frequency analysis of grounding systems considering the soil ionization effect," *IEEE Trans. Power Del.*, vol. 15, no. 1, pp. 103-107, Jan. 2000.

[13] A. F. Otero, J. Chdras and J. L. del Alamo, "Frequency-dependent grounding system calculation by means of a conventional nodal analysis technique," *IEEE Trans. Power Del.*, vol. 14, no. 3, pp. 873-878, Jul. 1999.

[14] J. He, R. Zeng, Y. Tu, J. Zou, S. Chen and Z. Guan, "Laboratory Investigation of Impulse Characteristics of Transmission Tower Grounding grids," *IEEE Trans. Power Del.*, vol. 18, no. 3, pp. 994-1001, Jul. 2003.

[15] N. M. Nor, A. Haddad, and H. Griffiths, "Characterization of ionization phenomena in soils under fast impulses," *IEEE Trans. Power Del.*, vol. 21, no. 1, pp. 353-361, Jan. 2006.

[16] N. M. Nor, A. Haddad, and H. Griffiths, "Performance of earthing systems of low resistivity soils," *IEEE Trans. Power Del.*, vol. 21, no. 4, pp. 2039-2047, Oct. 2006.

[17] D. Guo, D. Clark, D. Lathi, N.Harid, H.Griffiths, A. Ainsley, and A. Haddad, "Controlled Large-Scale Tests of Practical Grounding Electrodes - Part I Test Facility and Measurement of Site Parameters," *IEEE Trans. Power Del.*, vol. 29, no. 3, pp. 1231-1239, Jun. 2014.

[18] D. Clark, D. Guo, D. Lathi, N. Harid, H. Griffiths, A. Ainsley, and A. Haddad, "Controlled Large-Scale Tests of Practical Grounding Electrodes - Part II Comparison of Analytical and Numerical Predictions with Experimental Results," *IEEE Trans. Power Del.*, vol. 29, no. 3, pp. 1240-1248, Jun. 2014.

[19] W. C. Boaventura, I. J. S. Lopes, P. S. A. Rocha, R. M. Coutinho, F. Castro, and F. C. Dart, "Testing and Evaluating Grounding Systems of High Voltage Energized Substations: Alternative approaches," *IEEE Trans. Power Del.*, vol. 14, no. 3, pp. 923-927, Jul. 1999.

[20] K. Yamamoto, S. Yanagawa, K. Yamabuki, S. Sekioka, and S. Yokoyama, "Alternative Approaches Analytical Surveys of Transient and Frequency-Dependent Grounding Characteristics of a Wind Turbine Generator System on the Basis of Field Tests," *IEEE Trans. Power Del.*, vol. 25, no. 4, pp. 3035-3043, Oct. 2010.

[21] S. Visacro, R. Alipio, C. Pereira and M. Guimaraes, "Lightning Response of Grounding Grids Simulated and Experimental Results," *IEEE Trans. Electromagn. Compat.*, vol. 57, no. 1, pp. 121-127, Feb. 2015.

[22] A. Geri, G. M. Veca, E. Garbagnati, and G. Sartorio, "Non-linear Behaviour of Ground Electrodes Under Lightning Surge Currents: Computer Modelling and Comparison with Experimental Results," *IEEE Trans. magnetics*, vol. 28, no. 2, pp. 1442-1445, Mar. 1992.

[23] S. Sekioka, T. Sonoda, and A. Ametani, "Experimental Study of Current-Dependent Grounding Resistance of Rod Electrode," *IEEE Trans. Power Del.*, vol. 20, no. 2, pp. 1569-1576, Apr., 2005.

[24] C. H. Lee, C. N. Chang, and J. A. Jiang, "Evaluation of Ground Potential Rises in a Commercial Building During a Direct Lightning Stroke Using CDEGS," *IEEE Trans. Ind. Appl.*, vol. 51, no. 6, pp. 4882-4888, Nov., 2015.

[25] Z. Feng, X. Wen, X. Tong, H. Lu, L. Lan, and P. Xing, "Impulse Characteristics of Tower Grounding grids Considering Soil Ionization by the Time-Domain

Difference Method," *IEEE Trans. Power Del.*, vol. 30, no. 4, pp. 1906-1913, Aug. 2015.
[26] E. E. Oettle, "A new general estimation curve for predicting the impulse impedance of concentrated earth electrodes," *IEEE Trans. Power Del.*, vol. 3, no. 4, pp. 2020-2029, Oct. 1988.
[27] R. Alipio and S. Visacro, "Frequency Dependence of Soil Parameters: Effect on the Lightning Response of Grounding Electrodes" *IEEE Trans. Electromagn. Compat.*, vol. 55, no. 1, pp. 132-139, Feb. 2013.
[28] S. Visacro and R. Alipio, "Frequency Dependence of Soil Parameters: Experimental Results, Predicting Formula and Influence on the Lightning Response of Grounding Electrodes," *IEEE Trans. Power Del.*, vol. 27, no. 2, pp. 927-935, Apr. 2012.

Shuai Yang He received the B.Sc. degree in electrical engineering and automation from Wuhan University, in 2009, and the Ph.D. degree in high voltage and electrical insulation from Wuhan University, Wuhan, China, in 2014. From 2014 to 2018, he held a post-doctoral position at the School of Electrical Engineering, Wuhan University. Since 2018, he has been a Lecturer with the School of Electrical & Electronic Engineering, Hubei University of Technology, Wuhan, China. His research is mainly focused on high voltage and electrical insulation.

Jiarui Huang He received the B.Sc. degree in electrical engineering and automation from Hubei University of Technology, in 2014, and the M.S. degree in high voltage and electrical insulation from Wuhan University, Wuhan, China, in 2017. He is currently an engineer at China Electric Power Research Institute Co., Ltd., China.

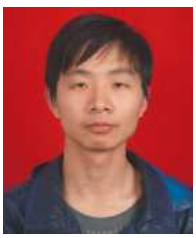

Shaodong Wei He received the B.Sc. degree in Mathematics and Applied Mathematics from Central South University, Changsha, China, in 2012, and the M.S. degree in high voltage and electrical insulation from Wuhan University, Wuhan, China, in 2015. He is currently an engineer at Hunan Provincial EHV Administration of Hunan Electric Power Corporation.

Wenjun Zhou He received the Ph.D. degree in 1990 from Wuhan University of Hydraulic & Electrical Engineering. Currently, he is a professor at the School of Electrical Engineering of Wuhan University, China. He is a member of the High Voltage Committee of the Chinese Society of Electrical Engineering (CSEE), the Electro-technical Test and Measurement Committee of the China Electro-technical Society (CES), and the China Lightning Protection Standard Committee. He is also the vice director of the Hubei High Voltage Committee. His research interests include lightning protection and the diagnostic techniques for outdoor electrical insulations